Journal of Optics

PAPER • OPEN ACCESS

Increasing the brightness of harmonic XUV radiation with spatially-tailored driver beams

OPEN ACCESS
IOP Publishing
Journal of Optics
J. Opt. **23** (2021) 015502 (7pp)
https://doi.org/10.1088/2040-8986/abcc56

Increasing the brightness of harmonic XUV radiation with spatially-tailored driver beams

D J Treacher[1], D T Lloyd[1], K O'Keeffe[2], F Wiegandt[1] and S M Hooker[1]

[1] Department of Physics, University of Oxford, Clarendon Laboratory, Parks Road, Oxford OX1 3PU, United Kingdom
[2] College of Science, Department of Physics, Swansea University, Singleton Park, Swansea SA2 8PP, United Kingdom

E-mail: k.okeeffe@swansea.ac.uk

Received 17 August 2020, revised 21 October 2020
Accepted for publication 19 November 2020
Published 14 December 2020

Abstract

Bright high harmonic sources can be produced by loosely focussing high peak power laser pulses to exploit the quadratic scaling of flux with driver spot size at the expense of a larger experimental footprint. Here, we present a method for increasing the brightness of a harmonic source (while maintaining a compact experimental geometry) by spatially shaping the transverse focal intensity distribution of a driving laser from a Gaussian to supergaussian. Using a phase-only spatial light modulator we increase the size and order of the supergaussian focal profiles, thereby increasing the number of harmonic emitters more efficiently than possible with Gaussian beams. This provides the benefits of a loose focussing geometry, yielding a five-fold increase in harmonic brightness, whilst maintaining a constant experimental footprint. This technique can readily be applied to existing high harmonic systems, opening new opportunities for applications requiring bright, compact sources of coherent short wavelength radiation.

Keywords: high-harmonic generation, frequency conversion, beam shaping

(Some figures may appear in colour only in the online journal)

1. Introduction

High harmonic generation (HHG) is an established method for producing highly coherent radiation in the XUV region with femtosecond to attosecond pulse durations [1]. However, the poor conversion efficiency of HHG from the infrared (IR) into the XUV typically restricts harmonic sources to average powers of a few microwatts or lower [2]. This limits their use in applications ranging from the production of isolated attosecond pulses [3] to lensless imaging [4, 5].

Increasing the average and peak fluxes of a harmonic source is of interest to experiments including photoelectron spectroscopy [6] and single-shot imaging [7]. The flux of a harmonic source can be increased through a variety of methods including phase matching [8], quasi-phase matching [9], as well as increasing the average power of the driver beam by increasing either the pulse energy or repetition rate, or both [10]. However, the most common and easily implemented approach is to increase the driver spot size by adopting a loose focussing geometry while also increasing the average power of the driving laser pulses [11]. For harmonics generated in a free-focus geometry by a driver beam with a spot size w_0 the harmonic energy E_h scales as $E_h \propto w_0^2$ [12]. Although the harmonic flux is sensitive to other parameters, such as the pulse duration, this quadratic scaling indicates that the focal length should be as long as possible in order to maximize the HHG flux. Although this approach offers a straightforward method for increasing the

flux of a harmonic beam, provided that the power of the driver beam can be increased sufficiently, it comes at the expense of increasing the experimental footprint, forfeiting one of the most attractive features of HHG sources.

An increase in either peak or average flux is most desirable when accompanied by a fixed or decreasing divergence. Satisfying these two conditions simultaneously is equivalent to increasing the brightness of a beam of radiation, defined as

$$B = \frac{\Phi}{\mathrm{d}\Omega \cdot A_s} \approx \frac{Nz^2}{\Delta t \cdot \pi w(z)^2 \cdot A_s}, \quad \forall z \gg w(z). \tag{1}$$

Here, $\Phi = N/\Delta t$ is the radiant flux (henceforth referred to as 'flux' for brevity) equivalent to the number of photons per unit time interval, A_s is the source size, $w(z)$ is the beam radius detected a distance z downstream and $\mathrm{d}\Omega$ is the solid angle subtended by the source. The beam parameter product (BPP), $\mathrm{d}\Omega \cdot A_s$, is conserved in an ideal optical system [13], and is a measure of the beam quality.

In this paper, we show that spatially shaping the transverse intensity profile of a driver laser at the focal plane can increase the harmonic brightness while maintaining a compact experimental footprint. The ideal transverse intensity distribution of the driver pulse would be a top-hat profile, since this corresponds to optimizing the fraction of the cross-section of the driving beam which is available to generate harmonics. However, it is challenging to create a perfect top-hat intensity profile (due to limitations described later in this paper), instead in this experiment a series of intermediate supergaussian profiles of increasing size and order were generated. Previously, supergaussain transverse intensity profiles have been created to drive harmonics using a focussing mirror with two optical paths [14, 15], and by passing the driving beam through two concentric glass plates [16]. Here we demonstrate the use of a spatial light modulator (SLM) to drive harmonics with a range of super-Gaussian transverse intensity profiles, with the programmable nature of the SLM providing a convenient method for tuning the intensity distribution at the focus. We show that a five-fold increase in harmonic brightness can be achieved without changing the focussing optics of the setup. This method, which can easily be applied to a wide range of existing HHG setups, enables the advantage of a loose focussing geometry to be realised while preserving a compact experimental footprint.

2. Experimental setup

In our implementation, shown in figure 1, the driver focal profile is transformed from Gaussian to a supergaussian profile by a phase-only SLM (Hamamatsu, X10468-02) with an active area comprising 792×600 square pixels of side 20 μm placed at the back focal plane of a lens with focal length $f = 0.5$ m. The profiles of the driving laser at the focus of the lens were measured by using a removable mirror to pass the driving laser beam through a 4-f unitary magnification reimaging line and onto a CCD camera which was mounted to a translation stage.

A gas cell with a longitudinal thickness of approximately 300 μm was located in the focal plane of the lens and backed with 50 mbar of argon. The longitudinal extent of the gas cell is significantly shorter than the Rayleigh range of the unshaped laser beams, minimizing phase-matching effects. This enabled us to attribute any change in brightness to the effects of our spatial shaping.

Following (1), the harmonic brightness can be determined by measuring the harmonic flux, divergence and source size. Of the three quantities the source size presents the greatest experimental challenge. In our case the source size was inferred by measuring the reimaged harmonic source. To achieve this, the primary harmonic source, of spot size $w_q^{(\mathrm{p})}$, at plane P was reimaged to the secondary source at plane S, with spot size $w_q^{(\mathrm{s})}$, as illustrated in figure 1. The reimaging was performed with a multilayer XUV focussing mirror with a focal length of 0.5m, magnification factor of 0.28 and reflectivity of 0.26 at $\lambda = (32 \pm 1.6)$ nm. The combination of Al filter and XUV focussing mirror resulted in the selection of a single harmonic order, corresponding to the 25th harmonic of the 800 nm driver beam, greatly simplifying the subsequent analysis. At plane S a knife-edge attached to a x–y–z nanopositioner (SmarAct SLC-1730) was used to measure $w_q^{(\mathrm{s})}$ directly, allowing $w_q^{(\mathrm{p})}$ to be determined. In the detector plane D, the harmonic signal was recorded by an x-ray CCD (Princeton Instruments, PIXIS-XO 400B) with a chip comprising 1340×400 square pixels of side 20 μm. The distance z between the S and D planes was calibrated from the diffraction pattern produced by the illumination of a double pinhole with known sizes, separation and wavelength, and found to be $z = (3.7 \pm 0.1)$ cm. This, together with the characterization of $w_q^{(s)}$ allows the divergence, and hence the BPP, of the harmonic beam to be determined. Ideally, the brightness of harmonic sources produced by a range of intermediate beam profiles between Gaussian and top-hat would be investigated. However, to produce an ideal top-hat driver field in plane P, the amplitude at the back focal plane of the lens should be proportional to a Bessel function of the first kind and order with π phase steps at each zero point in amplitude. In principle, such phase and amplitude shaping could be performed using two SLMs [17]. However, the increased complexity and cost of this approach, coupled with its inherent losses makes this impractical for HHG experiments, which require high peak laser intensity.

Here a single phase-only SLM is used, allowing simple, single parameter control of the beam shaping at pulse energies sufficient for HHG. The SLM was placed at the back focal plane of a lens and a single phase step of amplitude π and radius ρ was imprinted onto the collimated Gaussian driver, as shown schematically in the first plot inset in figure 1. The π phase shift causes the centre of the beam to interfere with the periphery of the beam at the focus, changing the intensity profile, as can be seen in the second plot inset in figure 1 for $\rho = 4.6$ mm. The resulting focal intensity distribution is seen to exhibit an approximately super-Gaussian profile, the width and exponent of which both vary with ρ. For the remainder of this paper, we plot results against the dimensionless quantity $\beta = w^{(\mathrm{slm})}/\rho$ where $w^{(\mathrm{slm})} = 4.3$ mm is the collimated driver beam radius measured at the plane of the SLM. When ρ is

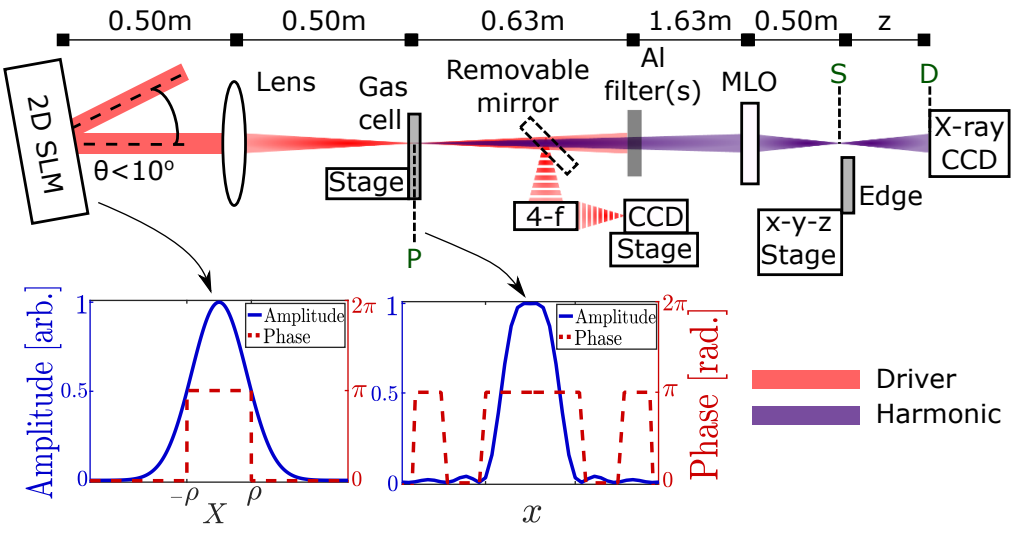

Figure 1. Beamline schematic. SLM is the phase-only spatial light modulator, P is the driver focal plane and primary harmonic source plane, 4-f is a unitary magnification reimaging line, MLO are multilayer optics that focus the harmonic beam to the secondary source plane S which is a distance z from the detection plane D. Left inset shows the amplitude (blue solid line) and phase (red dashed line) of the driver beam directly after the SLM. The right inset shows the corresponding driver amplitude and phase at the focal plane.

equal to the width of the SLM no shaping occurs since in this case the SLM simply acts as a plane mirror. In the following this case is denoted by $\beta = 0$.

We define a general supergaussian intensity profile as

$$I_{\mathrm{IR}}(x,y,n) = I_0 \exp\left[-2\left(\frac{\sqrt{(x-\bar{x})^2+(y-\bar{y})^2}}{w_0}\right)^n\right], \quad (2)$$

where, for a given n, the parameter w_0 determines the width of the beam, $(\bar{x},\bar{y})$ are the centre of mass coordinates of the profile in the transverse dimensions (x,y), and I_0 is the peak intensity. For a pulse with a Gaussian temporal profile with full width at half maximum duration τ and energy E_0, I_0 is

$$I_0 = \frac{4^{(1/n)}E_0}{\pi w_0^2 \Gamma\left[\frac{2+n}{n}\right]\cdot\tau}, \quad (3)$$

where Γ is the Gamma function [18]. For all results presented in this paper, the pulse energy was used to fix the peak focal intensity of each of the shaped driver beams at $I_0 = 4.7\times10^{14}$ W cm^{-2}. This intensity matched that of the unshaped Gaussian beam $I_{\mathrm{IR}}(x,y,2)$ with parameters; $w_0 = 34$ μm, $E_0 = 300$ μJ and $\tau = 35$ fs. For each profile the energy of the IR beam was measured using a powermeter (Ophir Model 30A-BB-18) and the pulse duration was measured using a GRENOUILLE (Swamp Optics Model 8-20-USB).

In figure 2(a) the measured values of w_0 and n of the shaped driver beam at the focal plane are shown for increasing values of β. The values were determined by performing a fit of the lineout through the centre of the beam profiles measured at the focus of the lens using (2) with n and ω_0 as free parameters. As the value of β increases the transverse intensity profile at the focus is modified from a Gaussian to supergaussian, resulting in an increase of both n and w_0. In figure 2(b) the measured intensity profiles at the focal plane are shown for three different values of β, together with fits of (2). Excellent agreement between the measured profiles and fits are observed up to $\beta = 0.93$. Beyond this value the measured transverse intensity distributions develop an on-axis minimum and are no longer accurately represented by super-Gaussians, as seen in figure 2(b) for $\beta = 1.02$. This breakdown in the desired beam shaping is reflected by the increasing error in n seen in figure 2(a) for $\beta > 0.93$. The emergence of an on-axis minimum for $\beta > 0.93$ is the result of destructive interference between the central and outer regions of the shaped driving laser which occurs as a result of performing phase-only shaping of the laser field. This could be avoided by shaping both the amplitude and phase of the driving laser, for example by using two SLMs at the expense of increasing the experimental cost and complexity. However, as can be seen in figure 2(a) using a single SLM already allows super-Gaussian orders up to $n = 3.75$ to be realised.

The conventional approach for increasing the harmonic flux by utilizing high f-number focussing optics corresponds to the case of increasing w_0 for fixed $n = 2$. However, in the shaping experiments described here both w_0 and n of the driving laser increase concomitantly for a fixed focusing optic.

3. Method

To demonstrate this approach the brightness of the harmonic beam was measured for five values of β. The brightness at each value was determined using (1) and the measured harmonic flux, as well as the beam size at the focus of the reimaged harmonic at plane S and the size of the harmonic beam at the detector plane D. The harmonic flux $\Phi = N/\Delta t$ was taken to be the spatially integrated counts recorded by the x-ray CCD in a time interval of 1 second. The value of $w(z)$ at the detector plane D was calculated using the second moment method [19]. A knife edge scan of the harmonic beam at plane S, assuming a

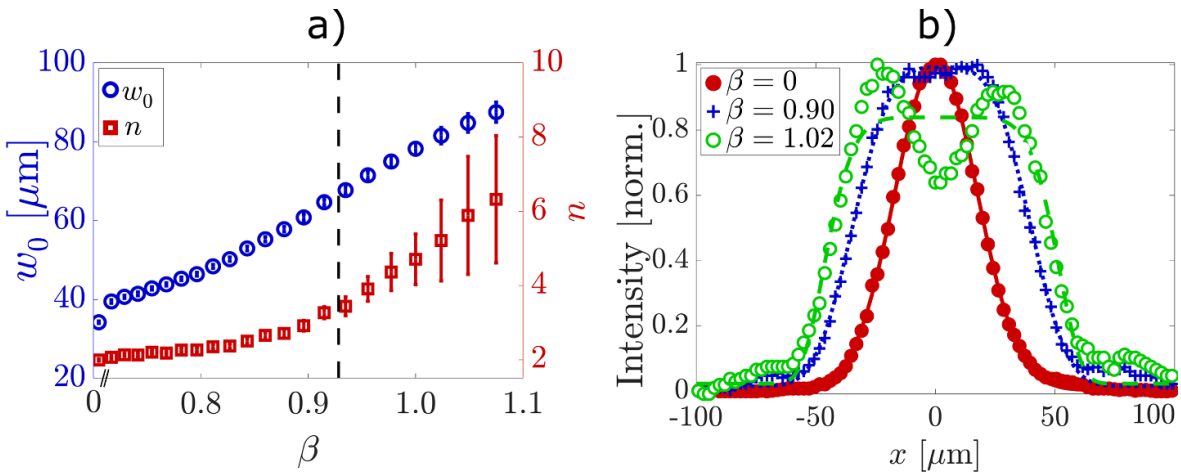

Figure 2. (a) The variation of the driver spot size w_0 (blue circles) and supergaussian order n (red squares) as a function of β. The vertical dashed line marks the onset of the deterioration in beam shaping. (b) Measured transverse intensity profiles of the focussed driver beam (symbols) for three different values of β. Also shown are fits of equation (2) (lines).

super-Gaussian harmonic intensity profile which is separable in x and y [18], was performed to determine $w_q^{(s)}$, and hence A_s. The location of plane S was determined by performing knife-edge measurements at multiple longitudinal positions.

The experimental set-up led to a small decrease in harmonic beam brightness as the beam propagated from the primary source to the detector plane due to absorption and wavefront distortions imposed by the XUV optics and filters. However, this reduction in brightness is independent of driver beam shaping. Hence, we report the *change* in the harmonic brightness as a result of shaping the driver beam, rather than the absolute brightness of the harmonic beam.

4. Results

Figure 3 shows the experimentally observed normalised harmonic flux as a function of β. A fivefold increase in flux is observed over the range of β values used, which is consistent with the fivefold increase in pulse energy required to maintain the same peak intensity over the range of β values investigated. The experimental data point at $\beta = 0.93$ highlighted by the shaded region in figure 3 is in the parameter region for which the shaped beam is not super-Gaussian, resulting in a decrease in harmonic flux.

Figures 4(a) and (b) show the harmonic beam profile recorded at plane D for $\beta = 0$ and $\beta = 0.9$, respectively. For $\beta = 0.9$, corresponding to the maximum super-Gaussian order that could be generated reliably in this experiment, the harmonic beam profile is clearly narrower than the case of the unshaped laser ($\beta = 0$). The lower divergence for $\beta = 0.9$ is due to the increased harmonic source size as a result of the larger width and lower transverse intensity variation of the shaped driving laser compared with the unshaped case. Figures 4(c) and (d) show the normalized lineouts through the centre of the profiles shown in figures 4(a) and (b), as well as the profiles simulated using the model discussed below.

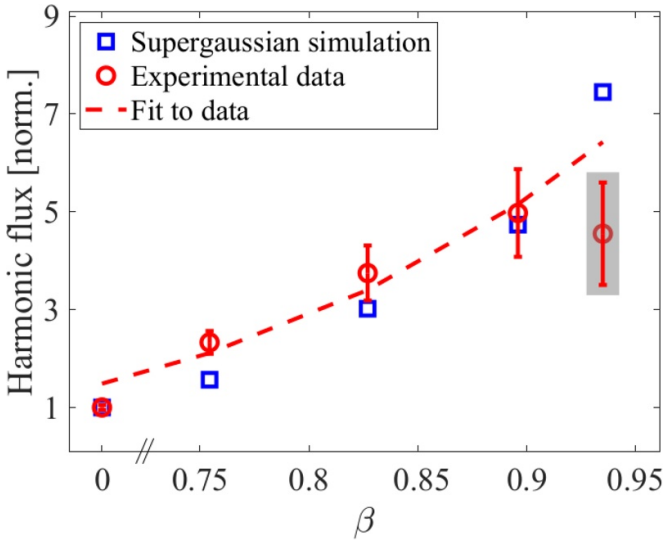

Figure 3. Measured (red circles) and simulated (blue squares) harmonic flux for the values of β investigated experimentally. The grey region indicates the data point at which beam shaping has deteriorated (i.e. $\beta > 0.93$) and is excluded from the fit to the data (red dashed line).

Reasonable agreement between the simulated and measured data is observed in both the shaped and unshaped cases.

Figure 5(a) shows the measured BPP and source size of the *reimaged* harmonics, $w_q^{(s)}$, as β is increased from 0 to 0.93. Over this range, w_0 from figure 2(a) increases by a factor of 1.98 ± 0.02, from 34 to 68 μm. However, the corresponding value of $w_q^{(s)}$ in figure 5(a) increases by a factor of 2.36 ± 0.26. The disparity between these two factors can be understood by considering that in the simple dipole model of high harmonic generation the amplitude of the harmonic field scales non-linearly with the driver amplitude, approximately as $\sqrt{I_0}^{q_{\text{eff}}}$, where q_{eff} is the effective non-linearity of the HHG interaction [20]. This scaling, together with (2), gives the relationship

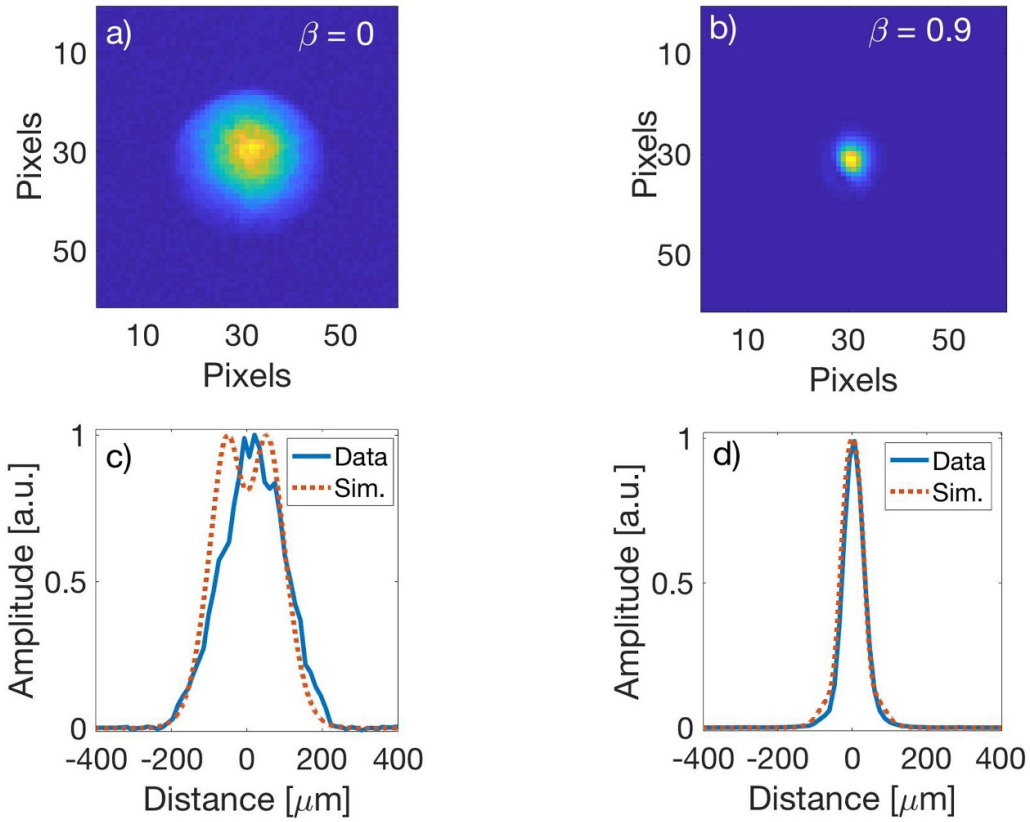

Figure 4. (a), (b) Harmonic beam profiles recorded at plane D for $\beta = 0$ and $\beta = 0.9$. (c), (d) Lineout through the centre of the recorded harmonic profile at plane D (solid blue line) and simulated beam profile (dotted orange line) for $\beta = 0$ and $\beta = 0.9$.

$$w_q^{(s)} = M \cdot \frac{w_0}{\sqrt[n]{q_{\text{eff}}}} \tag{4}$$

where M is the magnification of the reimaging system between planes P and S. Therefore, as both w_0 and n increase with β the harmonic source size increases more rapidly than the driver spot size, until the limit of a top-hot distribution is reached at which point the size of the driver and harmonic beams are equal.

Figure 5(a) shows that BPP is approximately independent of β. Hence, since the harmonic flux increases strongly with β, the brightness also increases with β, as shown in figure 5(b). However, $\beta = 0.93$ coincides with the region in figure 2(a) where the shaped beams are no longer supergaussian. In this case, as beam shaping breaks down the divergence of the harmonic beam was observed to increase rapidly causing the BPP to increase and hence the harmonic brightness to decrease.

The measured brightness of the harmonic beam for each value of β is shown in figure 5(b). The highest brightness recorded was a factor of 5 ± 0.65 larger than the unshaped $I_{\text{IR}}(x, y, 2)$ driver profile, having doubled w_0 without changing the focussing optic. In maintaining a fixed peak laser intensity, the laser pulse energy was increased by a factor of 4.8 for the situation where the highest improvement in brightness was recorded. The increase in flux and approximately constant BPP for $\beta < 0.93$, shown in figures 3 and 5(a) respectively, satisfy the two requirements for increasing the brightness of the harmonic beam, as outlined at the beginning of this paper. We note that over the range of values of β where the desired beam shaping could be achieved it was demonstrated that the BPP was independent of the supergaussian order. As a result, the same improvement in brightness could also have been achieved by approximately doubling the focal length of the focussing optic while maintaining the same peak intensity at focus, however, this approach comes at the expense of increasing the experimental footprint. Alternatively, a similar brightness could be achieved through a five-fold increase in the repetition rate of the driving laser, while maintaining the same pulse energy. However, since many laser systems operate at a fixed repetition rate, this approach is often not feasible.

We note that the main source of error in our results arise from uncertainties in the knife edge measurements of $w_q^{(s)}$. These uncertainties are minimal when $\beta = 0$ ($n = 2$) because in this case the SLM acts as a planar mirror such that small variations in the driver pointing have a negligible effect on the primary (and therefore reimaged) harmonic source(s). However, for $\beta > 0$, the SLM imprints a spatially-dependent phase, and hence small variations in driver pointing create a large skew in the intensity profile of the driver at the focal plane. This skew causes a linear phase gradient in the primary harmonic source term, resulting in a shift of the transverse position of the reimaged harmonic source. Hence, for $\beta > 0$ jitter in the pointing of the driver will cause larger uncertainties in the values of $w_q^{(s)}$ compared to the case of $\beta = 0$. We note this could be minimised by implementing a beam-pointing stabilization system.

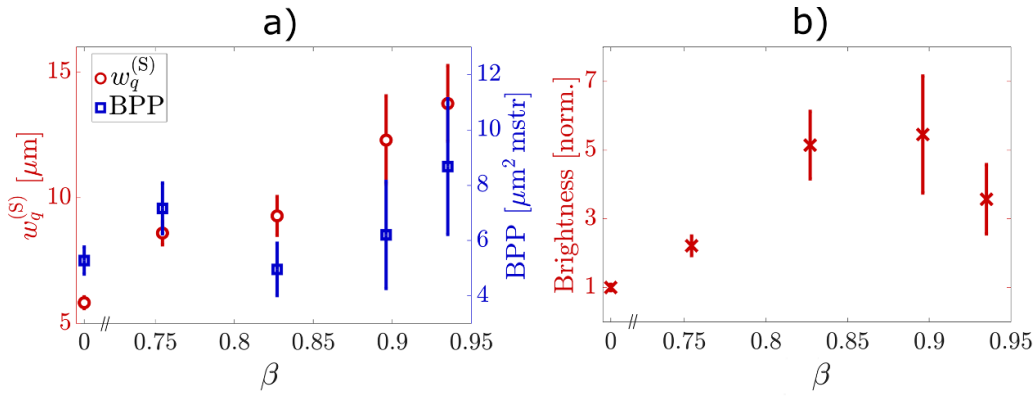

Figure 5. (a) Measured $w_q^{(s)}$ (red open circles) and BPP (blue open squares) as a function of β. (b) Measured harmonic brightness as a function of β.

The phase of harmonic emission is given by $\phi_q = q\phi_{IR} + \phi_{at}$, where ϕ_{IR} is the phase of the driving laser and ϕ_{at} is the atomic dipole phase. To assess the impact of transverse phase variations on our results a range of supergaussian driver profiles were numerically propagated through the focal region using the angular spectrum method (ASM). For all of the profiles considered it was found that the transverse variation of ϕ_{IR} was less than 0.05 radians within the gas cell, such that ϕ_{IR} can be considered constant within the interaction region. Using the simple dipole model of HHG the complex field of the q^{th} harmonic order in plane P is then given by $E_q^{(p)} \propto \sqrt{I_{IR}}^{q_{\mathrm{eff}}} e^{-i\phi_{\mathrm{at}}}$, where $\phi_{\mathrm{at}} \approx \alpha_q^j I_{IR}$ and α_q^j is a proportionality constant depending on the jth electron trajectory [20]. In our experimental arrangement only the short trajectory component ($j = s$) is considered since the more divergent long trajectory components lie outside the acceptance angle of the imaging system. For $I_0 = 4.7 \times 10^{14}$ W cm^{-2}, and $q = 25$, a value of $\alpha_{25}^{\mathrm{s}} = 1.04 \times 10^{-14}\,\mathrm{cm}^2\,\mathrm{W}^{-1}$ was calculated using the method described in [20] and a value of $q_{\mathrm{eff}} = 2.6$ was determined using (4). Using the simple dipole model the resulting harmonic fields were calculated for a range of super-Gaussian profiles and propagated to the detector plane using ASM. It was found that ϕ_{at} had a negligible effect on the rate of change of beam divergence as a function of super-Gaussian order.

The flux of the generated harmonics was also calculated for the same values of β used in the experiment by spatially integrating the harmonic source terms in the simple dipole model described above, where in each case I_{IR} was taken as the fit to the corresponding measured intensity profile using (2). The results are compared with the measured data in figure 3. Good agreement between the measured and simulated flux is observed in regions where beam shaping could be performed effectively ($\beta < 0.93$). Beyond this the measured harmonic flux no longer increases with β due to the deterioration in beam shaping. The simulated data shown in figure 3 indicates that higher flux could be achieved than was realised in this experiment, provided the super-Gaussian transverse profiles of the driver beam could be maintained at higher values of β and sufficient laser energy was available. We note that in order to achieve higher order super-Gaussians than demonstrated in this work, both amplitude and phase shaping of the driving laser would be required. For example, static plates with high damage thresholds could be designed to include the concentric phase steps and amplitude shaping not implemented in this paper, at the expense of not being able to continuously vary the intensity distribution at the focal plane. We note also that the flux of the harmonic source could be further increased by employing phase matching techniques as previously discussed by Constant *et al* [14]. For the experiments presented here the shaped transverse profiles could be maintained over a longitudinal region of approximately 1 mm. Provided phase matching can be achieved over this distance it would be possible to increase the flux further through careful optimization of the thickness of the gas cell.

5. Conclusion

In this paper we have shown that by spatially shaping the intensity distribution of a driver beam at the focal plane from a Gaussian to super-Gaussian, a five-fold increase in the brightness of a high harmonic beam could be realised. The brightness increase shown in this paper was achieved without changing the driver focussing optics, therefore maintaining a highly compact experimental footprint. The ease of implementing the method described in this paper opens the door to its immediate application to experiments which require high brightness, low divergence short wavelength radiation such as coherent ultrafast imaging.

Acknowledgments

The authors acknowledge financial support from Engineering and Physical Sciences Research Council (EP/N029313/1, EP/L015137/1); F Wiegandt was supported by H2020 Marie Skłodowska-Curie Actions (641272).

ORCID iD

K O'Keeffe https://orcid.org/0000-0003-2085-0806

References

[1] Gaarde M B, Tate J L and Schafer K J 2008 Macroscopic aspects of attosecond pulse generation *J. Phys. B: At. Mol. Opt. Phys.* **41** 27

[2] Falcão-Filho E L, Lai C J, Hong K H, Gkortsas V M, Huang S W, Chen Li J and Kärtner F X 2010 Scaling of high-order harmonic efficiencies with visible wavelength drivers: a route to efficient extreme ultraviolet sources *Appl. Phys. Lett.* **97** 061107

[3] Vincenti H and Quéré F 2012 Attosecond lighthouses: how to use spatiotemporally coupled light fields to generate isolated attosecond pulses *Phys. Rev. Lett.* **108** 113904

[4] Treacher D J, Lloyd D T, Wiegandt F, O'Keeffe K and Hooker S M 2019 Optimised xuv holography using spatially shaped high harmonic beams *Opt. Express* **27** 29016–25

[5] Abbey B *et al* 2011 Lensless imaging using broadband x-ray sources *Nat. Photon* **5** 420–4

[6] Chiang C T, Huth M, Trutzschler A, Kiel M, Schumann F O, Kitschner J and Widdra W 2015 Boosting laboratory photoelectron spectroscopy by megahertz high-order harmonics *New J. Phys.* **17** 013035

[7] Ravasio A *et al* 2009 Single-shot diffractive imaging with a table-top femtosecond soft x-ray laser-harmonics source *Phys. Rev. Lett.* **103** 028104

[8] Popmintchev T, Chen M C, Bahabad A, Gerrity M, Sidorenko P, Cohen O, Christov I P, Murnane M M and Kapteyn H C 2009 Phase matching of high harmonic generation in the soft and hard x-ray regions of the spectrum *Proc. Natl Acad. Sci.* **106** 10516–21

[9] Wiegandt F, Anderson P N, Yu F, Treacher D J, loyd D T, Mosley P J, Hooker S M and Walmsley I A 2019 Quasi-phase-matched high-harmonic generation in gas-filled hollow-core photonic crystal fiber *Optica* **6** 442–7

[10] Wang H, Xu Y, Ulonska S, Robinson J S, Ranitovic P and Kaindl R A 2015 Bright high-repetition-rate source of narrowband extreme-ultraviolet harmonics beyond 22 eV *Nat. Commun.* **6** 7459

[11] Rudawski P *et al* 2013 A high-flux high-order harmonic source *Rev. Sci. Instrum.* **84** 073103

[12] Rothhardt J, Krebs M, Hädrich S, Demmler S, Limpert J and Tünnermann A 2014 Absorption-limited and phase-matched high harmonic generation in the tight focusing regime *New J. Phys.* **16** 033022

[13] Wang Z, Segref A, Koenning T and Pandey R 2011 Fiber coupled diode laser beam parameter product calculation and rules for optimized design *Proc. SPIE* **7918** 791809

[14] Constant E, Dubrouil A, Hort O, Petit S, Descamps D and Mével E 2012 Spatial shaping of intense femtosecond beams for the generation of high-energy attosecond pulses *J. Phys. B: At. Mol. Opt. Phys.* **45** 074018

[15] Dubrouil A, Mairesse Y, Fabre B, Descamps D, Petit S, Mével E and Constant E 2011 Controlling high harmonics generation by spatial shaping of high-energy femtosecond beam *Opt. Lett.* **36** 2486–8

[16] Boutu W *et al* 2011 High-order-harmonic generation in gas with a flat-top laser beam *Phys. Rev.* A **84** 063406

[17] Haotong M, Zhou P, Wang X, Yanxing M, Xi F, Xu X and Liu Z 2010 Near-diffraction-limited annular flattop beam shaping with dual phase only liquid crystal spatial light modulators *Opt. Express* **18** 8251–60

[18] Andrews L C 1998 *Special Functions of Mathematics for Engineers* (Oxford: Oxford Science Publications)

[19] Siegman A E 1998 How to (maybe) measure laser beam quality *DPSS (Diode Pumped Solid State) Lasers: Applications and Issues* MQ1

[20] Catoire F *et al* 2016 Complex structure of spatially resolved high-order-harmonic spectra *Phys. Rev.* A **94** 063401